Proceedings of the 1st Marine Energy Technology Symposium
METS13
April 10-11, 2013, Washington, D.C.

Hydrodynamic Design and Optimization of Hydro-kinetic Turbines using a Robust Design Method

Nitin Kolekar[1] Zhen Hu[2] Arindam Banerjee[1,a] Xiaoping Du[2]
[1]Department of Mechanical Engineering & Mechanics, Lehigh University, Bethlehem, PA 18015
[2]Department of Mechanical and Aerospace Engineering, Missouri S&T, Rolla, MO 65409
[a] Corresponding author: arb612@lehigh.edu

ABSTRACT

Hydro-kinetic Turbines (*HKT*)*, unlike conventional hydraulic turbines are zero head energy conversion devices, which utilize the kinetic energy of flowing water for power generation. The performance of these turbines depends on various parameters like number of blades, tip speed ratio, type of airfoil, blade pitch, chord length & twist and its distribution along the blade span. The present work aims at maximizing the performance of a horizontal axis hydrokinetic turbine through a coupled computational fluid dynamics-blade element momentum* (*hydrodynamic*) *analysis. Optimization is carried out using both robust and deterministic-design optimization schemes and comparison is presented. The current analysis is focused on constant chord blades due to low cost and ease of fabrication. A hydrodynamic analysis is carried out using blade element momentum (BEM) theory to study effect of various operating parameters on forces and torque developed by the turbine, thereby arriving at optimized design with maximum performance coefficient. BEM code is validated with experimental data from NREL phase III rotor. BEM analysis is compared with a detailed three-dimensional computational fluid dynamics (CFD) analysis. Finally, CFD analysis results are presented for optimized geometry.*

Nomenclature:

a = axial induction factor
a' = angular induction factor
B = number of blades
$BEM(\mathrm{x})$ = BEM function for optimization
C_d = actual drag coefficient (based on Re)
$C_{d,\,ref}$ = drag coefficient based on Re_{ref}
c = chord length [m]
C_{p} = performance coefficient
dQ & dT = torque & thrust developed on a blade element at radius r [N & N.m]
F_{Hub} & F_{Tip} = hub loss & tip loss correction factors
m = optimization target
$m_{C_{oe}}$ = mean value of performance coefficient
m_c, m_{TSR}, $m_{\theta_{po}}$ = mean values of chord lengths TSR and blade pitch angles
P = Turbine Power
$\boldsymbol{p}_{\mathbf{r}}$ = vector of random parameters
R = turbine radius [m]
Re = flow Reynolds number
Re_{ref} = reference Reynolds number for hydrodynamic data input
$R(m_{\mathbf{x}_r})$ = robustness metrics
r = radius of blade element [m]
r_{hub} = hub radius [m]
U = flow velocity [m/s]
$\vec{U}_r$ = relative flow velocity in rotating reference frame [m/s]
$s^2_{C_{oe}}$ = standard deviation of C_{p}
$\boldsymbol{x}_{\mathbf{d}}$ = vector of deterministic design variables
$\boldsymbol{x}_{\mathbf{r}}$ = vector of random design variables
∇p = pressure gradient across the turbine [N/m^2]

μ = dynamic viscosity of water [Pa.s]
ω = angular velocity of the wake [rad/s]
Ω = turbine rotational speed [rad/s]
ϕ = angle of relative flow [°]
ρ = water density [kg/m^3]
σ = local blade solidity
σ_{C_p} = standard deviation of C_p
θ_{po} = blade pitch angle [°]

1.0 INTRODUCTION

Renewable energy resources are gaining global attention due to depleting fossil fuels and harmful environmental effects associated with their usage. Hydro, wind, solar, biomass and geothermal energies form the bulk of renewable energy sources; among which hydro power offers one of the most exciting and sustainable proposition. Traditionally, hydropower has accounted for the bulk of the renewable energy production in the United States. The primary energy use in the U.S. in 2011 was 28,516 TWh/yr of which only 9% came from renewables[1]. Traditional hydroelectric or micro-hydro facilities contributed 35% of total renewable energy production[1]. However, growth of conventional hydropower plants are limited due to limitations on the number of available natural sites, large capital (initial) investment, pay-back time and environmental concerns. In lieu of this, marine and hydrokinetic (MHK) systems offer many advantages: these are portable systems with small initial cost, no large infrastructure and easy and quick deployment [2-5]. A study conducted by Electric Power Research Institute (EPRI) for US rivers estimated hydrokinetic power potential of 12,500 MW[6, 7]. This study was based on conservative assumption of turbine array deployment for rivers with discharge rates greater than 113 m^3/s and flow velocities greater than 1.3 m/s. A study conducted by EPRI evaluated many, but not all tidal energy sites in U.S. and estimated 115 TWh/yr of tidal energy[6, 7]. These estimates show potential of MHK systems.

Hydrokinetic turbines (HKT) are a class of low head energy conversion devices which convert kinetic energy of flowing water into mechanical work[8, 9]. Tidal and marine current turbines also falls into similar category of (lift-drag) devices which utilize hydrodynamic blade shapes to derive power from flowing fluid. Depending on the flow direction of water relative to the axis of rotation, HKT can be classified as horizontal axis and vertical axis turbines. The performance of these turbines is governed by the three non-dimensional parameters defined below: (a) tip-speed ratio (TSR) that is defined as the ratio of blade tip speed to fluid speed; (b) solidity (σ) that is defined as the ratio of blade chord length times the number of blades to turbine circumference; and, (c) Reynolds number.

$$TSR = \frac{R\Omega}{U} \quad (1)$$

$$\sigma = \frac{Bc}{2\pi R} \quad (2)$$

$$\mathrm{Re} = \frac{\rho U c}{\mu} \quad (3)$$

Over the last decade, the hydrodynamics of HKT has been investigated using computational fluid dynamics (CFD) [10-12] and laboratory scale experiments [13-15]. Blade-element-momentum (BEM) analysis which forms the backbone of wind turbine rotor design can be used for HKT design [16]. Apart from BEM, a series of inexpensive CFD tools based on the solution of the Euler or Navier-Stokes equations like panel method and vortex lattice method can be used for aerodynamic/hydrodynamic analysis of these devices [17]. In addition, computationally expensive techniques that involve solving Reynolds-averaged-Navier-Stokes equations (RANS) with turbulence models has been successfully used for hydrodynamic analysis of HKT[10, 12, 18].

Consul *et al.*[10] performed a two dimensional CFD analysis to understand the influence of number of blades on performance of cross flow turbines and found improved performance with higher number of blades. Higher solidity turbine performed better at low tip speed ratios and low angles of attack[10]. Duquette and co-workers[12] performed experiments and 2-D numerical analysis to study the effect of number of blades and solidity on the performance of horizontal axis wind turbine. The numerical analysis was performed using BEM and lifting

line based wake theory[12]. Their analysis concluded that the range of TSR for maximum C_p depends strongly on solidity and weakly on number of blades. This suggests that the chord length decides the optimum TSR range of the turbine. Their laboratory experiments with micro-turbines with flat plate blades showed that larger blade pitch angles tend to decrease the optimum TSR range significantly with small change in maximum C_p. Myers and Bahaj [13-15] experimentally investigated the flow field and wake recovery behind tidal turbine using mesh disk simulators and found that recovery depends on proximity to water surface, sea bed roughness(which governs vertical velocity profile and turbulent kinetic energy of flow) and to a lesser extent on rotor thrust. Mukherji *et al.*[18] performed detailed three-dimensional CFD to understand effect of TSR, solidity, blade pitch and number of blades on performance of HKT. They reported a strong influence of TSR on performance coefficient for various turbine geometries. Performance coefficient is a ratio of turbine power to the available power in the flowing fluid passing through rotor swept area (Equation 4).

$$C_p = \frac{Turbine\ power}{water\ power} = \frac{P}{\frac{1}{2}\rho A U^3} \qquad (4)$$

Further, increase in turbine solidity and blade numbers were reported to maximize the C_p with maximum C_p observed at lower TSR.

The knowledge base derived from aerodynamic/hydrodynamic analysis of wind/hydrokinetic turbines can be used for further design optimization study. Most of the optimization studies for wind turbines[19-21] were focused on maximizing coefficient of performance and annual energy production (AEP). Selig and Coverstone-Carroll[19] used a genetic algorithm (GA) for optimizing AEP and cost of energy of low-lift airfoils for stall regulated wind turbines (wind turbines that have their blades designed so that when fluid speeds are high, the rotational speed or the torque, and thus the power production, decreases with increasing fluid speed above a certain value that is usually not the same as the rated speed). Belesis[20] presented GA for constrained optimization of stall regulated wind turbine and found it to be superior to classical optimization methods. Fuglsang and Madsen[21] performed multi-disciplinary optimization on stall regulated horizontal axis wind turbine considering fatigue, maximum load and AEP. Most of these studies were based on BEM analysis and did not consider three dimensional flow dynamics which is inherent to wind turbines and hydrokinetic turbines.

The present work focuses on maximizing the performance of a stall regulated, fixed pitch, constant chord, horizontal axis hydrokinetic turbine operating in a cavitation free environment that is sufficiently away from the free-surface by using a combination of BEM and three dimensional CFD analysis. As a starting point, a hydrodynamic analysis is carried out using BEM theory; the objective being to study the effect of various operating parameters on torque developed by the turbine. BEM(lower order-analytical model = less physics) results are compared with a detailed three-dimensional CFD analysis (higher order model = more physics) to test the fidelity of BEM analysis. Aerodynamic data for BEM parametric study is obtained from Xfoil[22]. Results of parametric study were used as a guideline for setting up bounds on decision variables (TSR, c, θ_{po}) during optimization process. Optimization was performed using robust design approach to handle uncertainties in nondeterministic variables: river velocity, angle of attack of river flow, and rotational speed of turbine. Also, the robust design results are compared with deterministic design approach. The optimized geometry is then modeled in ANSYS CFX and a three-dimensional computational fluid dynamics (CFD) analysis is performed to calculate the fluid forces and torque developed by turbine. This provides validation for our BEM based optimization approach.

2.0 THEORY AND APPROACH:

BEM theory, originally attributed to Betz and Glauert[16] is a combination of blade element theory and momentum theory. According to blade element theory, forces on turbine blade can be obtained by dividing blade into number of aerodynamically (or hydrodynamically) independent elements.

Aerodynamic forces on these elements are calculated based on local flow conditions using two dimensional lift-drag data. Forces are then summed together to find total force on turbine blade. Momentum theory, the other half of BEM assumes that the work done by the flow on turbine blade creates pressure (or momentum) loss across the rotor plane. Induced velocities in axial and tangential direction can be calculated from this momentum loss. These induced velocities affect the forces on turbine blade. BEM combines blade element and momentum theory and solves coupled equations in iterative manner to determine fluid forces (thrust and torque) and induced velocities near rotor[23]. The original BEM theory of Betz and Glauert was modified for our HKT analysis to take into account effect of hub, tip and Reynolds number dependence for aerodynamic/hydrodynamic data correction. Prandtl's tip loss correction factor was incorporated in the algorithm to account for losses due to fluid flow from pressure side to suction side at blade tip as:

$$F_{Tip} = \frac{2}{\pi}\cos^{-1}\left(\exp\left(\frac{B(r-R)}{2r\sin(\phi)}\right)\right) \quad (5)$$

The hub loss correction factor was also incorporated to account for losses caused by swirling flow due to presence of hub as:

$$F_{Hub} = \frac{2}{\pi}\cos^{-1}\left(\exp\left(\frac{B(r_{hub}-r)}{2r_{hub}\sin(\phi)}\right)\right) \quad (6)$$

The effects of correction factors for tip and hub losses are combined into single factor F that is defined as:

$$F = F_{Tip} \times F_{Hub} \quad (7)$$

The tip and hub loss correction factor is used to determine net thrust and torque from turbine:

$$\left.\begin{aligned} dT &= F\rho U^2 4a(1-a)\pi r dr \\ dQ &= 4Fa'(1-a)\rho U\pi r^3\Omega dr \end{aligned}\right\} \quad (8)$$

The axial induction factor (a) is defined as fractional decrease in water velocity between the free stream and the rotor plane. The angular induction factor (a') is defined as one half the ratio of the angular velocity of the wake to the angular velocity of the rotor (a' = $\omega/2\Omega$). Lift and drag coefficients for SG6043 hydrofoil that were adopted for our HKT blades are obtained from Xfoil[22]. Xfoil calculates lift and drag forces on a given hydrofoil by combining a linear-vorticity stream function panel method and a viscous solution method (for boundary layer and wake). The entire viscous solution is strongly interacted with the incompressible potential flow via the surface transpiration model. Aerodynamic data obtained from Xfoil is corrected according to Equation 9 suggested by Hernandez and Crespo[24] as:

$$C_d = C_{d,\mathrm{Re}_{\mathrm{Ref}}}\left(\frac{\mathrm{Re}_{\mathrm{Ref}}}{\mathrm{Re}}\right)^{0.2} \quad (9)$$

that suggests that the drag coefficient scales inversely with Reynolds number but the lift coefficient remains relatively unchanged. Eq. 9 should be used with extreme caution as it is based on small wind turbines over a Reynolds no. range of 10^5 to 10^7 and represents a very simplistic approach. Estimation of the drag coefficients at low values of Reynolds number can be very complex.

2.1 Computational Fluid Dynamics analysis:

A three-dimensional CFD analysis was performed where Reynolds Averaged Navier-Stokes equations (RANS) were solved in ANSYS CFX using a multiple reference frames technique [25]. A rotating reference frame was incorporated to take into account the effect of turbine rotation by transforming an unsteady flow in an inertial (stationary) frame to a steady flow in a non-inertial (moving) frame using equations below:

$$\nabla\cdot\vec{U}_r = 0 \quad (10)$$

$$\rho\left[\frac{\partial}{\partial t}(\vec{U}_r) + \nabla\cdot(\vec{U}_r\vec{U}_r) + (2\vec{\Omega}\times\vec{U}_r + \vec{\Omega}\times\vec{\Omega}\times\vec{r})\right] = -\nabla p + \nabla\cdot\tau_r \quad (11)$$

where $\vec{U}_r$ is the relative velocity viewed from rotating reference frame, $\vec{\Omega}$ is the rotational speed of the turbine, $\rho(2\vec{\Omega}\times\vec{U}_r)$ is the Coriolis force, $\rho(\vec{\Omega}\times\vec{\Omega}\times r)$ is the centrifugal force, τ_r is viscous stress tensor, ∇p is the pressure gradient across the turbine. The fluid domain consists of inner rotating domain with turbine and outer stationary domain as shown in Figure 1. A grid independence study was carried out to study effect of number of elements on the CFD analysis. Mesh size was varied from a coarser mesh of 3.5 million to a finer mesh of 10 million elements and flow variables were monitored.

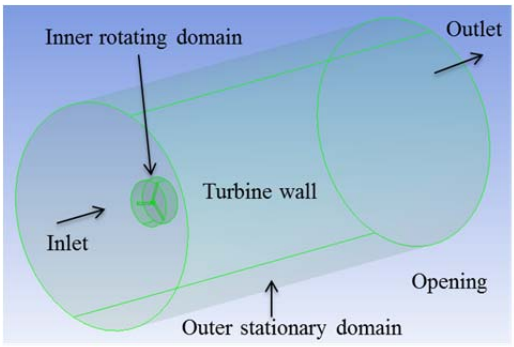

Figure 1 Computation domain and mesh used for CFD analysis

A mesh with 7.8 million elements was found to be optimal, as increasing mesh size beyond this point did not cause appreciable change in torque and forces on turbine. Mesh was locally refined with prism elements on turbine wall for accurate boundary layer prediction to attain a y+ value <100. A y+ value is a non-dimensional parameter related to mesh size which defines distance of first mesh node from the turbine wall where a no-slip boundary condition is imposed. Lower the y+, better the boundary layer flow resolved near the wall[26]. Convergence criteria for continuity and momentum equations were set to 10^{-6} absolute and higher order numerics were used for turbulence modeling. A *k-ω* SST (Shear Stress Transport) turbulence model was chosen due to its accuracy for adverse pressure gradient flows as the current case [27-29].

2.2 Robust Design Optimization:

To account for uncertainties inherent in the working environment of HKT, optimization is carried out using both deterministic and robust design approaches. The considered uncertainties include variation in river velocity, chord length, pitch angle and TSR. Table 1 summarizes parameters and design variables used for optimization. Out of eight input parameters, four are deterministic parameters (turbine radius, hub radius, number of blades and number of blade elements), water velocity is a random parameter, and the other three are random design variables (pitch angle, TSR, and chord length). The mean values of random design variables are expected to be optimized to maximize the power coefficient. Water velocity is truncated at [0.8, 3.7] m/s based on average river flow data[30, 31] and chord length is truncated at six sigma level to account for manufacturing tolerances. Equation 12 presents the robust design model used for the optimization study.

$$\min R\left(m_{x_r}\right);\ C_{oe} = BEM(\boldsymbol{p}_d, \boldsymbol{p}_r, \boldsymbol{x}_d, \boldsymbol{x}_r)$$
$$0.03 \le m_c \le 0.18 \quad ; \quad 2 \le m_{TSR} \le 12 \quad ;$$
$$0° \le m_{\theta_{po}} \le 18° \qquad (12)$$

where, $R(m_{\mathbf{x}_r})$ is the robustness metrics, $BEM(\mathrm{x})$ is the BEM function with inputs of $\mathbf{p_d}$, $\mathbf{p_r}$, $\mathbf{x_d}$, and $\mathbf{x_r}$, $\mathbf{p_d}$ =[*R, r*$_{hub}$*, B, N*] is the vector of deterministic parameters, $\mathbf{p_r}$ =[*U*] is the vector of random parameters, $\mathbf{x_d}$ =[ ] is the vector of deterministic design variables, and $\mathbf{x_r}$ =[θ_{po}*, TSR, c*] is the vector of random design variables whose mean values need to be optimized. The robustness matrix used for the current study is given by

$$R = w_1(m_{C_{oe}} - m)^2 + w_2 s^2_{C_{oe}},\ w_1 + w_2 = 1 \qquad (13)$$

where, m is the target of optimization, $m_{C_{oe}}$ is the mean value of performance coefficient, $s^2_{C_{oe}}$ is the standard deviation of performance coefficient, w_1 and w_2 are weights for optimization. The mean value and standard deviation of performance coefficient is obtained from Monte Carlo Simulation (MCS) for current study. The values of weights, w_1 and w_2, represent the decision maker's preference to the mean value and variance. For example, if the mean value is more important than the variance to the decision maker, then a larger value is assigned to the weight w_1. On the other hand, if the variance is more important, a larger value is then assigned to w_2. A Pareto curve represents the points of mean value and variance under different combinations of w_1 and w_2. From the Pareto curve, if designers prefer a large mean value, they will then sacrifice the variance; and vice versa if they prefer a large variance value.

2.3 Validation of BEM with Experimental data:

Due to absence of experimental data for our HKT design, BEM code was validated with NREL phase III combined experimental rotor (CER) results[32] . NREL CER rotor is a 5.03m radius, three bladed wind turbine having

varying chord, twisted blades. This turbine uses S809 airfoil from blade root to blade tip. BEM analysis was carried out over a range of blade pitch angles (0 to 7°) and TSR (0 to 8). Figure 2a-c compares results of BEM with NREL data, which shows a good match up to TSR values of 5. At high TSR values, BEM analysis deviates from experiments which can be attributed to non-uniform blade loading[33] and accelerated span-wise flow, which are not taken into account in BEM analysis.

Table 1. Parameters and design variables used for the optimization study

Parameter	Type	Mean Value	Standard deviation
Turbine radius (R)	Deterministic	1m	0
Hub radius (r_{hub})	Deterministic	0.1m	0
# of blades (B)	Deterministic	3	0
# of blade elements (N)	Deterministic	20	0
Water velocity (U)	Truncated Gaussian	2m/s	0.4 m/s
Blade pitch angle (θ_{po})	Uniform	$m_{\theta_{po}}$	$\left[m_{\theta_{po}} - 1°, \quad m_{\theta_{po}} + 1° \right]$
TSR	Uniform	m_{TSR}	$[\, m_{TSR} - 0.2, \quad m_{TSR} + 0.2]$
Chord length (c)	Truncated Gaussian	m_c	5×10^{-3}

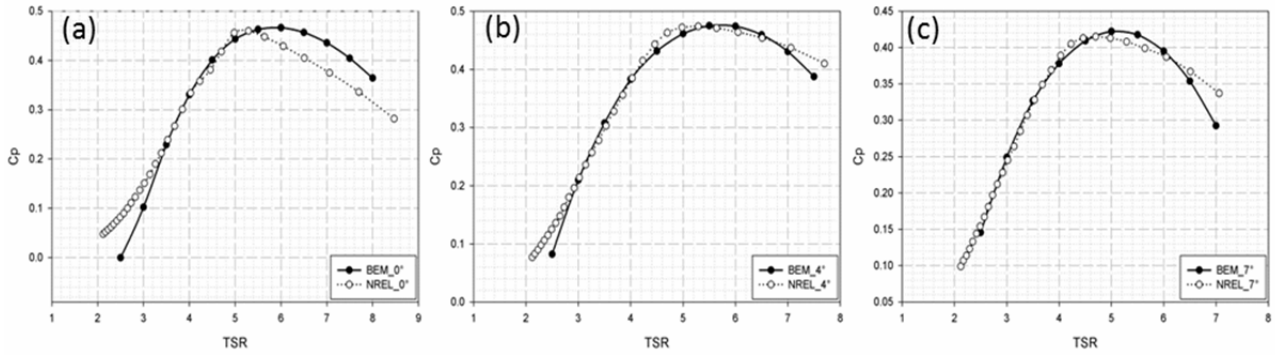

Figure 2 Validation of BEM with NREL experiments: (a) 0° blade pitch, (b) 4° blade pitch, (c) 7° blade pitch

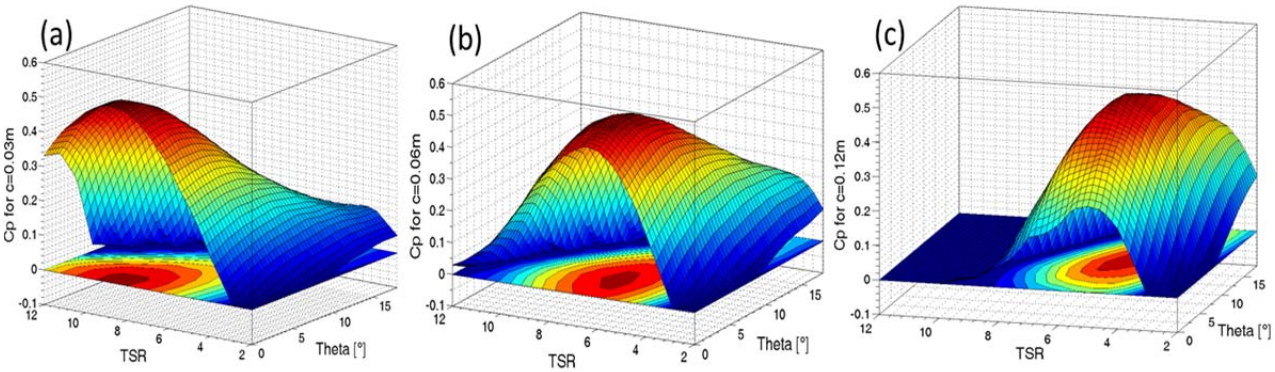

Figure 3 Effect of TSR and blade pitch angle on turbine performance at various chord lengths: (a) 0.03m chord, (b) 0.06m chord, (c) 0.12m chord

3.0 RESULTS AND DISCUSSION:

a. BEM parametric study:

A validated BEM code was used for hydrodynamic analysis of a model three-bladed constant chord turbine of radius 1m. This turbine uses SG6043 airfoil from root to tip as it gives a high C_L/C_d value over the current operating range of Reynolds number ($1\times10^5<Re<5\times10^5$) [12, 34, 35]. BEM analysis is performed to understand effect of chord length, blade pitch and TSR on the turbine performance. The turbine blade was divided into 20 elements and BEM analysis was performed to estimate thrust forces and

torque developed on the turbine blades. The water velocity used for analysis was 2 m/s which is considered average river water velocity in the U.S. [30]. The design space selected for current study is such that TSR is varied from 2 to 12, blade pitch angle from 0° to 18° and chord length from 0.015 to 0.18m. The experience gained from wind turbine industry is used to specify TSR range for parametric study. For a wind turbine, which is a lift-drag device similar to HKT, the TSR for maximum C_p ranges from 6 to 10. The SG6043 airfoil used for current study, depending on flow Reynolds number, has stall angle around 14°-16°. Hence the design parameter space of [0°, 18°] is expected to cover all possible operating blade pitch angles for optimizing C_p. The lower limit on chord-length is based on manufacturing feasibility and upper limit of 0.18m was specified to restrict R/c to 0.56(σ=0.086). Higher the chord length, larger the blade area undergoing thrust loading which is detrimental to turbine life. Further, increase in chord length does not improve the performance significantly but only shifts C_p vs TSR curve towards origin[12, 18]. The results of the parametric study are presented in Figure 3a-c showing the effect of blade pitch and TSR on turbine performance coefficient for blades with chord lengths of 0.03m, 0.06m, and 0.12m respectively. As the chord length is increased from 0.03 (Figure 3a) to 0.12m (Figure 3c), the bell shaped C_p vs TSR curve shifts towards the origin; which implies that higher the chord length, lower is the TSR for maximum performance. In addition, higher the chord length, higher the blade pitch angle for maximum performance. Furthermore, for a given chord length, lower the TSR, higher the blade pitch for maximum performance. In general, hydrodynamic analysis suggests that, lower values of blade chord lengths maximize the coefficient of performance.

b. Optimized results:

Taking a cue from parametric study, optimization was carried out using deterministic design and robust design approaches to maximize the performance of model HKT. Figure 4 illustrates the Pareto curve of robust design optimization of hydrokinetic turbine blades. Figure 4 shows that the standard deviation of C_p will increase with the mean value of C_p. A larger C_p corresponds to a larger standard deviation. Thus, designer can make a decision to achieve a tradeoff between mean and standard deviation. The optimized design variables and turbine blade performance from deterministic design and robust design are given in Table 2. In this paper, we use w_1=0.78 and w_2=0.22. The target for optimization, *m* is assigned a value of 0.6.

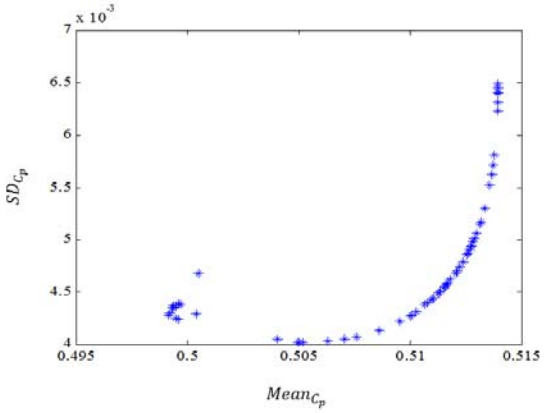

Figure 4 Pareto curve of robust design.

The results illustrate that the deterministic design method can achieve a maximum C_p of 0.52, but its mean value is a smaller than that of robust design and its standard deviation is about two times of that of robust design. The robust design has a smaller TSR than the deterministic design. The comparison of PDFs of C_p under deterministic design and robust design is shown in Figure 5.

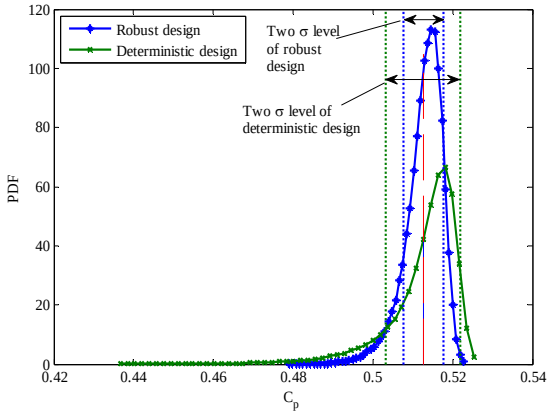

Figure 5 Comparison of Probability Density Functions (PDFs) from deterministic design and robust design

The two sigma level and mean value of the two PDFs are also indicated in Figure 5. The figure demonstrates that design from robust design method has a smaller standard deviation and larger mean value. Hence, the robust design method is less sensitive to the uncertainties in working environment than the deterministic design. The two sigma level of PDF under deterministic design is much larger than that of robust design as shown in Figure 5.

Table 2. Optimized results of deterministic design and robust design

[Note: m_{C_p} , $C_{p,\max}$ and s_{C_p} are mean, maximum and standard deviation of performance coefficient]

Method	θ_{po}	TSR	c	m_{C_p}	s_{C_p}	$C_{p,\max}$
Deterministic Design	2.06	7.75	0.039	0.5126	0.0093	0.52
Robust Design	3.92	6.36	0.059	0.5127	0.0049	0.517

c. CFD analysis:

This section summarizes results of three-dimensional CFD analysis performed in ANSYS CFX using a rotating reference frame technique [18]. CFD analysis was performed to test the fidelity of BEM based optimization technique. The turbine geometries with different blade configurations (blade pitch angle and chord lengths) were modeled in SolidWorks and meshing was carried out in ANSYS. A hybrid mesh with 7.8 million elements having prism layers on turbine wall was used for CFD analysis. The results of CFD analysis are summarized and compared with BEM analysis in Table 3.

Table 3 Comparison of BEM with CFD analysis

Variables			CFD		BEM	
Blade Pitch (°)	**Chord (m)**	**TSR**	**Thrust (N)**	C_p	**Thrust (N)**	C_p
10	0.12	4.0	4753	0.45	4832	0.42
12	0.12	4.0	4241	0.42	4403	0.43
13.5	0.14	3.1	3627	0.35	3881	0.36
14.4	0.14	3.5	3817	0.38	4121	0.39
6.9	0.1	6.9	8134	0.33	6577	0.35

The CFD results agree in principle with values obtained from BEM analysis. The discrepancy in thrust and C_p values can be attributed to simplified assumptions of BEM theory which states that the forces acting on blade element are essentially two-dimensional (calculated based on aerodynamic data). Moreover, BEM does not take into account hydrodynamic interaction between adjacent blade elements and the effect of vortices generated at blade tip, blade trailing edge and blade root. These vortices affect the flow field around turbine and hence the performance of turbine.

The CFD results for robust-optimized geometry are compared with BEM analysis in Table 4. The coefficient of performance and thrust force on turbine obtained from CFD are comparable to those obtained from BEM validating the results of our optimization. The tip vortices, centrifugal and Coriolis forces acting along the blade affect the flow field and performance of the turbine. CFD analysis takes into account all these effects which are not modeled in BEM analysis.

Table 4 Comparison of CFD with BEM analysis

[Note: All parameters are in SI units.]

Blade pitch	**Chord**	**TSR**	**BEM**		**CFD**	
			C_p	**Force**	C_p	**Force**
3.92	0.059	6.36	0.51	5667	0.45	5609

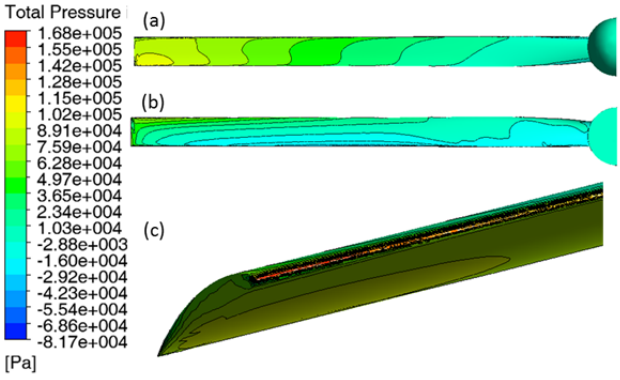

Figure 6 Total pressure contours on turbine blade on: (a) Pressure side, (b) Suction side, (c) Zoomed in view of leading edge.

The contours of total pressure(in stationary frame) on pressure side(upwind) and suction side(downwind) of the blade are shown in Figure 6. On the pressure side(Figure 6a) , the part of blade near the tip experience higher pressure compared to rest of the span. Similarly, on suction side(Figure 6b) lower pressure is observed near the blade tip compared to the part of the blade near the hub. Thus the pressure gradient across the blade is higher at regions away from the blade root. The blade region away from the hub is subjected to successively higher relative water velocity and higher angle of relative flow. This indicates that the part of blade away from root contributes more towards hydrodynamic forces and has significant role in thrust and torque development. Figure 6c shows zoomed in view of total pressure contour near leading edge of blade which shows the presence of stagnation zone near the leading edge and not far into the pressure side of blade. This indicates that the angle of relative flow (sum of angle of attack and blade pitch angle) is still below stall point.

The CFD analysis demonstrates possibilities of further improvement in hydrodynamic performance. The contribution of near hub blade region can be improved by providing higher pitch angles near the blade root. A twisted blade with successively decreasing section pitch angles from blade root to tip will not only improve Cp, but will help achieving uniform loading on blade. While the current work focused on a constant chord blade HKT, the future work will target hydro-structural optimization based on coupled BEM-CFD-FE (finite element) analysis.

4.0 CONCLUSION:

A hydrodynamic analysis and optimization based on robust design methodology shows that the performance of hydrokinetic turbine can be maximized by choosing the right combination of design variables. Coefficient of performance as high as 0.52 was achieved with a constant chord blade turbine in a non-cavitating environment at depths sufficiently away from the free surface. Results of BEM are in reasonable agreement with three dimensional steady state CFD analysis. Robust design method yielded a design configuration which is less susceptible to uncertainties in design variables than the deterministic design.

ACKNOWLEDGEMENT:

The authors gratefully acknowledge the support from the Office of Naval Research through contract ONR N000141010923.

REFERENCES:

1. *Annual Energy Review*, in *Office of Energy Statistics, U.S. Energy Information Administration*. 2011: Washington, DC 20585.
2. Hall, D.G., et al., *Water Energy Resources of the United States with Emphasis on Low Head/Low Power Resources*, I.N.E. Laboratory and Environmental, Editors. 2004, U.S. Department of Energy.
3. Hall, D.G., et al., *Wind and Hydropower Technologies, Feasibility Assessment of the Water Energy Resources of the United States for New Low Power and Small Hydro Classes of Hydroelectric plants, Tech report-DOE-ID-11263*, in *U.S. Department of Energy, Energy Efficiency and Renewable Energy*. 2006, Idaho National Laboratory.
4. Date, A. and A. Akbarzadeh, *Design and Cost Analysis of Low Head Simple Reaction Hydro Turbine for Remote Area Power Supply.* Renewable Energy, 2009. **34**: p. 409-415.
5. Guney, M.S. and K. Kaygusuz, *Hydrokinetic Energy Conversion Systems: A Technology Status Review.* Renewable and Sustainable Energy Reviews, 2010. **14**(9): p. 2996-3004.
6. Bedard, R., *Overview of U.S. Ocean Wave and Current Energy: Resource, Technology, Environmental and Business Issues and Barriers*. 2007: Electric Power Research Institute.
7. Bedard, R., *Prioritized Research, Development, Deployment and Demonstration Needs: Marine and Other Hydrokinetic Renewable Energy*. 2008, Electric Power Research Institute.
8. Khan, M.J., M.T. Iqbal, and J.E. Quaicoe, *River Current Energy Conversion Systems: Progress, Prospects and Challenges.* Renewable and Sustainable Energy Reviews, 2008. **12**: p. 2177-2193.
9. Schwartz, S.S., *Proceedings of the Hydrokinetic and Wave Energy Technologies Technical and Environmental Issues Workshop*, ed. I.

Prepared by Resolve. 2006, Washington, D.C.: Office of Energy Efficiency and Renewable Energy, U.S. Department of Energy.
10. Consul, C.A., et al. *Influence of Solidity on the Performance of a Cross-flow Turbine*. in *Proceedings of the 8th European Wave and Tidal Energy Conference*.
11. Duquette, M.M. and J. Swanson, *Solidity and Blade Number Effects on a Fixed Pitch, 50W Horizontal Axis Wind Turbine.* Wind Engineering, 2003. **27**(4): p. 299-316.
12. Duquette, M.M. and K.D. Visser, *Numerical Implications of Solidity and Blade Number on Rotor Performance of Horizontal Axis Wind Turbines.* Journal of Solar Energy Engineering, 2003. **125**: p. 425-432.
13. Myers, L. and A.S. Bahaj, *Wake Studies of a 1/30th Scale Horizontal Axis Marine Current Turbine.* Ocean Engineering, 2007. **34**: p. 758-762; 758.
14. Myers, L. and A.S. Bahaj, *Power Output Performance Characteristics of a Horizontal Axis Marine Current Turbine.* Renewable Energy, 2006. **31**: p. 197-208.
15. Myers, L.E. and A.S. Bahaj, *Experimental Analysis of the Flow Field around Horizontal Axis Tidal Turbines by use of Scale Mesh Disk Rotor Simulators.* Ocean Engineering, 2010. **37**(2–3): p. 218-227.
16. Glauert, H., *Airplane Propellers*, in *Aerodynamic Theory* W.F. Durand, Editor. 1935, Berlin:Springer Verlag.
17. Sørensen, J.N., *Aerodynamic Aspects of Wind Energy Conversion.* Annual Review of Fluid Mechanics, 2011. **43**(1): p. 427-448.
18. Mukherji, S.S., et al., *Numerical Investigation and Evaluation of Optimum Hydrodynamic Performance of a Horizontal Axis Hydrokinetic Turbine.* Journal of Renewable and Sustainable Energy, 2011. **3**: p. 063105.
19. Selig, M.S. and V.L. Coverstone-Carroll, *Application of a Genetic Algorithm to Wind Turbine Design.* Journal of Energy Resources Technology, 1996. **118**(1): p. 22-28.
20. Belessis, M.A., D.G. Stamos, and S.G. Voutsinas. *Investigation of the Capabilities of a Genetic Optimization Algorithm in Designing Wind Turbine Rotors*. in *Proc. European Union Wind Energy Conf. and Exhibition*.
21. Fuglsang, P. and H.A. Madsen, *Optimization Method for Wind turbine Rotors - A New Dual Method using Mixed Variables.* Journal of Wind Engineering and Industrial Aerodynamics, 1999. **80**(1): p. 191-206.
22. Mark, D. and Y. Harold. *XFoil, Subsonic Airfoil Development System*. [cited 2012 08/15]; Available from: http://web.mit.edu/drela/Public/web/xfoil/.
23. Manwell, J.F., J.G. McGowan, and A.L. Rogers, *Wind Energy Explained: Theory, Design and Application*. Vol. 2nd. 2009, New York: John Wiley and Sons.
24. Hernandez, J. and A. Crespo, *Aerodynamics Calculation of the Performance of Horizontal Axis Wind Turbines and Comparison with Experimental Results.* 1987. **11**(4): p. 177-187.
25. *ANSYS CFX 12.0.1 User's guide*. 2010, ANSYS, Inc.
26. Wilcox, D.C., *Turbulence Modeling for CFD*. 3rd ed. 2006, La Canada, CA: DCW Industries.
27. Menter, F.R., *Two-equation Eddy-Viscosity Turbulence Models for Engineering Applications.* AIAA Journal, 1994. **32**(8): p. 1598-1605.
28. Menter, F.R., *Performance of Popular Turbulence Models for Attached and Separated Adverse Pressure Gradient Flows.* AIAA Journal, 1992. **30**(8): p. 2066-2072.
29. Vermeer, L.J., J.N. Sorensen, and A. Crespo, *Wind Turbine Wake Aerodynamics.* Progress in Aerospace Sciences, 2003. **39**: p. 467-510.
30. Parkinson, G.V., *Phenomena and modeling of flow-induced vibrations of bluff bodies.* Progress in Aerospace Science, 1989. **26**: p. 169-224.
31. Neary, V.S. and D.C. Sale, *Flow characteristics of river resources for hydrokinetic energy conversion.*, in *Hydrovision 2010*. 2010: Charlotte, NC. .
32. Giguère, P. and M.S. Selig, *Design of a Tapered and Twisted Blade for the NREL Combined Experiment Rotor*. 1999, NREL: Golden, Colorado.
33. Madsen, H.A., et al., *Validation and Modification of the Blade Element Momentum Theory based on Comparisons with Actuator Disc Simulations.* Wind Energy, 2010. **13**(4): p. 373-389.
34. Hu, Z., et al., *Robust Design with Imprecise Random Variables and its Application in Hydrokinetic Turbine Optimization.* Engineering Optimization, 2013(To appear).
35. Giguère, P. and M.S. Selig, *New Airfoils for Small Horizontal Axis Wind Turbines.* ASME Journal of Solar Energy Engineering, 1998. **120**: p. 108-114.